iScience

CellPress
OPEN ACCESS

Article

# Quantum interference probed by the thermovoltage in Sb-doped $Bi_2Se_3$ nanowires

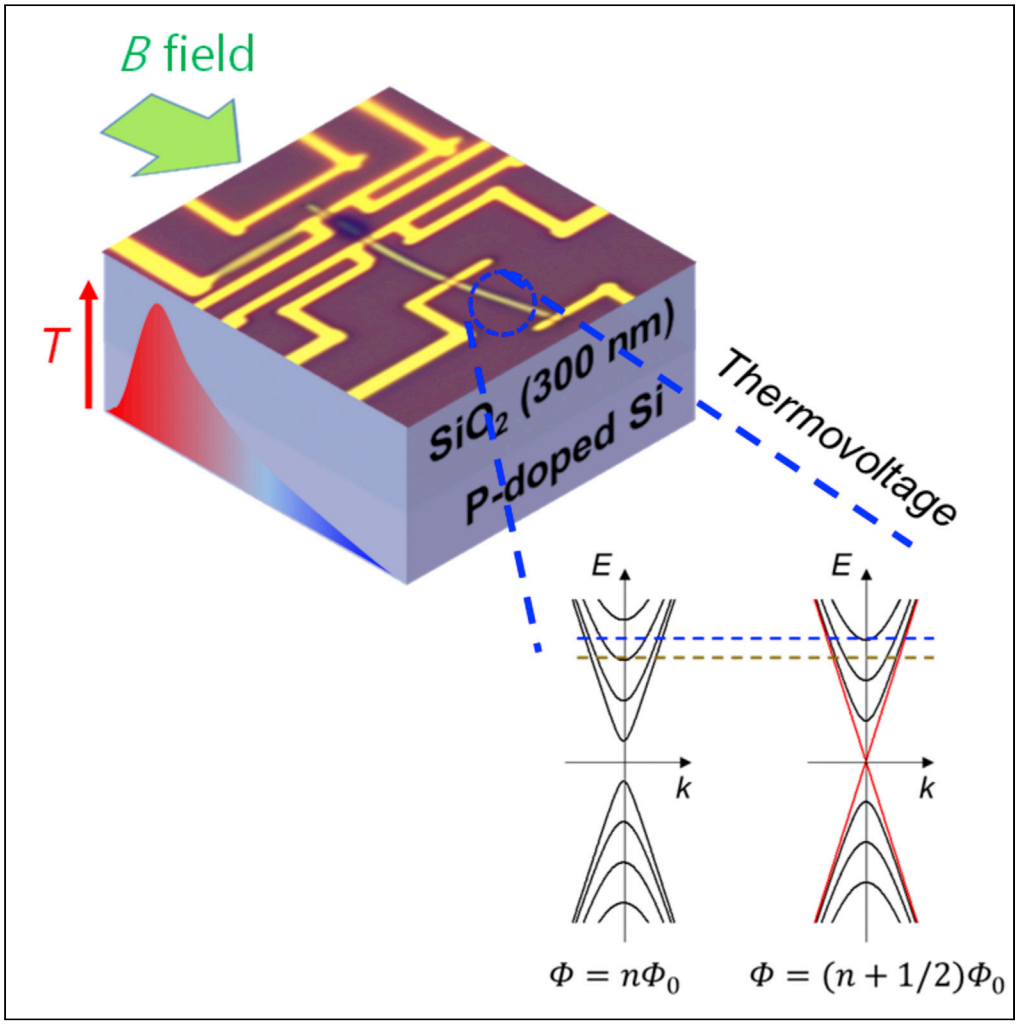


Duhyuk Kwon, Bum-Kyu Kim, Yong-Joo Doh, Dong Yu, Jonghyun Song, Myung-Ho Bae

songjonghyun@cnu.ac.kr (J.S.)
mhbae@kriss.re.kr (M.-H.B.)

## Highlights

Aharonov–Bohm interference in topological insulator nanowires probed by thermovoltage

180° out-of-phase thermovoltage oscillations with the magnetic flux and gate voltage

Thermoelectric signal as a probe of electronic structure in quantum materials

Kwon et al., iScience 26, 105691
January 20, 2023 
https://doi.org/10.1016/j.isci.2022.105691

iScience

CellPress
OPEN ACCESS

Article

# Quantum interference probed by the thermovoltage in Sb-doped $Bi_2Se_3$ nanowires

Duhyuk Kwon,[1,2] Bum-Kyu Kim,[2] Yong-Joo Doh,[3] Dong Yu,[4] Jonghyun Song,[1,6,*] and Myung-Ho Bae[2,5,7,*]

## SUMMARY

**The magnetic-flux-dependent dispersions of sub-bands in topologically protected surface states of a topological insulator nanowire manifest as Aharonov–Bohm oscillations (ABOs) observed in conductance measurements, reflecting the Berry's phase of $\pi$ because of the spin-helical surface states. Here, we used thermoelectric measurements to probe a variation in the density of states at the Fermi level of the surface state of a topological insulator nanowire (Sb-doped $Bi_2Se_3$) under external magnetic fields and an applied gate voltage. The ABOs observed in the magnetothermovoltage showed 180° out-of-phase oscillations depending on the gate voltage values, which can be used to tune the Fermi wave number and the density of states at the Fermi level. The temperature dependence of the ABO amplitudes showed that the phase coherence was kept to $T = 15$ K. We suggest that thermoelectric measurements could be applied for investigating the electronic structure at the Fermi level in various quantum materials.**

## INTRODUCTION

Thermoelectric (TE) studies of low-dimensional nanostructures have been extensively carried out to achieve a high figure of merit for the energy conversion between electricity and heat.[1–5] After the discovery of topological insulator (TI) properties of traditional TE materials such as bismuth selenide ($Bi_2Se_3$) and bismuth (antimony) telluride [$Bi_2(Sb_2)Te_3$], many theoretical and experimental approaches have been performed to improve the TE properties using the TI surface states.[6–11] However, the experimental approach to investigate the electronic structure based on the TE effect has not been intensively investigated. Because the Seebeck coefficient ($S$) or thermovoltage ($V_{ThV} = -S\Delta T$, where $\Delta T$ is the temperature difference between two spatially separated points) is sensitive to the electronic density of states (DOS) at the Fermi level, measurements of $V_{ThV}$ can provide information about the electronic structure near the Fermi level.[12–14]

In the present study, we report magnetothermovoltage measurements for an Sb-doped $Bi_2Se_3$ (BiSe) nanowire (NW) under axial magnetic flux ($\Phi$). Pronounced oscillations with varying $\Phi$ were observed in both the magnetothermovoltage and the magnetoconductance with the same period satisfying the Aharonov–Bohm oscillation (ABO). The thermovoltage as a function of gate voltage showed 180° out-of-phase oscillations for the two cases of $\Phi = 0$ and $\pm\Phi_0/2$, where $\Phi_0$ is the magnetic flux quantum. The magnetothermovoltage oscillations also showed the 180° out-of-phase behavior at the local maximum and minimum locations in the gate-dependent oscillation obtained at $\Phi = 0$ or $\pm\Phi_0/2$. These results are consistent with the $\Phi$-dependent sub-band dispersion model for the topologically protected surface states of a TI NW, which has been mainly demonstrated by the ABO in the magnetoconductance. The results reflect the sensitivity of the thermovoltage to the change of the DOS at the Fermi level under a varying gate voltage and varying magnetic field; thus, the thermovoltage measurement could be a useful tool to study the electronic structure of various quantum materials.

## RESULTS AND DISCUSSION

### Electrical characterization

Figure 1A shows an optical image of a Sb-doped BiSe NW device (BiSe#1) fabricated on a 300 nm-thick $SiO_2$/Si substrate using conventional microfabrication processes. The device has four metal (Ti/Au) contacts and three NW segments for the electrical and thermovoltage measurements and a heater line to

[1]Department of Physics, Chungnam National University, Daejeon 34134, Republic of Korea

[2]Korea Research Institute of Standards and Science, Daejeon34113, Republic of Korea

[3]Department of Physics and Photon Science, Gwangju Institute of Science and Technology, Gwangju61005, Korea

[4]Department of Physics, University of California at Davis, Davis, CA95616, USA

[5]Department of Nano Science, University of Science and Technology, Daejeon, 34113, Republic of Korea

[6]Institute of Quantum Systems (IQS), Chungnam National University, Daejeon34134, Republic of Korea

[7]Lead contact

*Correspondence: songjonghyun@cnu.ac.kr (J.S.), mhbae@kriss.re.kr (M.-H.B.)

https://doi.org/10.1016/j.isci.2022.105691

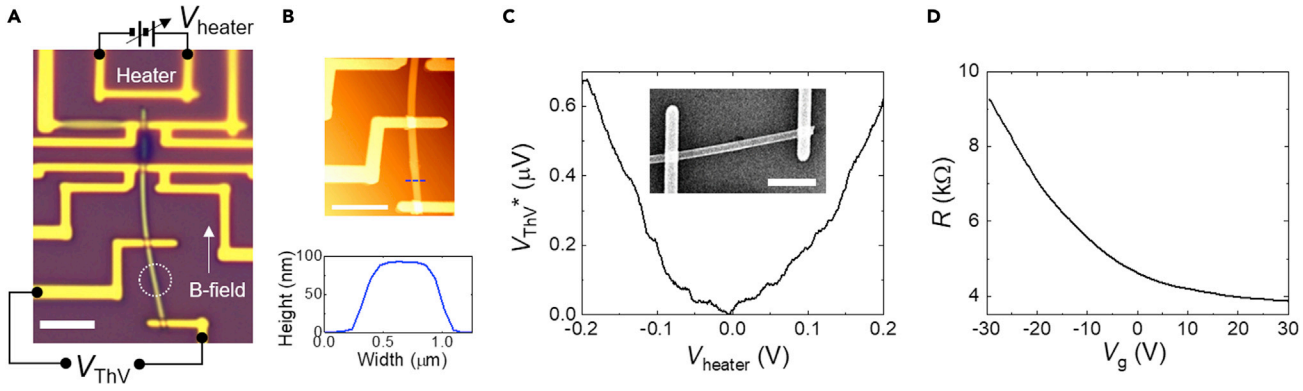


**Figure 1. Device images and electrical characterization**

(A) Optical image of the Sb-doped $Bi_2Se_3$ NW device (BiSe#1) configured for the thermovoltage measurement. Scale bar: 5 μm. The bottom NW segment denoted by a dashed circle was used in the present study.

(B) Upper and lower panels: Atomic force microscopy (AFM) image and the height profile along the dashed blue line in the upper panel, respectively. Scale bar: 5 μm.

(C) Thermovoltage ($V_{ThV}$*) as a function of heater voltage ($V_{heater}$). Inset: Scanning electron microscope (SEM) image of the device. Scale bar: 3 μm.

(D) Resistance ($R$) as a function of the gate voltage ($V_g$).

apply a temperature gradient along the NW (see STAR Methods for details of the fabrication and measurements). The highly doped Si substrate served as a gate electrode. The thermovoltage measurement configuration is also shown in the image. In the present study, we used the bottom segment of the NW [length ($L$) = 6.8 μm, width ($W$) = 440 nm, height ($H$) = 93 nm], as denoted by a dashed circle, because the topmost NW segment having two metallic thermometers was burnt during measurements and the second metal contact from the top could have been deformed by the burning. Here, the height and width of the NW were obtained from an AFM image (see Figure 1B) and SEM image (see the inset of Figure 1C), respectively. Although the third contact was as far as 13 μm from the heater line, we observed a measurable $V_{ThV}$* as a function of the voltage applied to the heater ($V_{heater}$) at $T$ = 4.2 K (Figure 1C), where $V_{ThV}$* is a thermovoltage after subtracting a minimum voltage from the raw data in Figure S1A in the Supplementary Information. The $V_{ThV}$*-$V_{heater}$ plot shows nearly symmetric behavior for the polarity of the $V_{heater}$, which is evidence of a thermoelectric signal.[15] Figure 1D displays the resistance ($R$) as a function of the back-gate voltage ($V_g$), which shows that an $n$-type carrier is the dominant carrier for the examined $V_g$ region.

## Aharonov–Bohm oscillations in magnetoconductance and magnetothermovoltage

In Figure 2, we investigate the conductance ($G$) and thermovoltage ($-V_{ThV}$) under an applied magnetic ($B$) field at $V_g$ = 0 V and $T$ = 4.2 K with BiSe#1, where the $B$ field was applied parallel to the axial direction of the first segment of the NW from the top in Figure 1A. The NW examined in the present study (indicated by the dotted circle in Figure 1A) was misaligned with the $B$-field direction by as much as ~13°. Here, we used the thermovoltage as $-V_{ThV}$ to match the polarity to the Seebeck coefficient $S$. The black curve in the upper panel of Figure 2A displays $G$ as a function of the $B$ field (top axis)-; the curve shows that the conductance decreases with increasing $B$ field in both polarities, resulting in a sharp peak near zero $B$ field. This result indicates the existence of weak antilocalization (WAL) because of the spin–orbit interaction in the bulk.[16,17] A relatively small magnetoconductance modulation superimposed on the WAL curve of the smooth fitting result (the red curve in the upper panel of Figure 2A) was observed. The lower panel of Figure 2A shows a pronounced oscillation in $\Delta G$ as a function of the $B$ field, where $\Delta G$ was obtained by subtracting the smooth fitting result from the raw data (black curve). From a fast Fourier transformation (FFT) analysis (Figure 2B), we obtained the oscillation period as $\Delta B$ = 0.112 T, which is consistent with that estimated from a TI NW with a measured geometry of $W$ = 430 nm and $H$ = 83 nm when a 5 nm-thick oxidized layer of the TI NW was assumed to be present and the angle was tilted with respect to the $B$-field direction, following the ABO.[18–21] This result indicates that the magnetoconductance oscillation observed in the TI NW is related to the surface state of the NW. The lower horizontal axis is $\Phi$ in the unit of $\Phi_0$ (=$h/e$), where $h$ and $e$ are Planck's constant and the elementary charge, respectively. Although the conductance maxima in the oscillation are located at integer multiples of $\Phi_0$ for $-5 < \Phi < 5$, the oscillation phase continuously evolves with increasing $B$ fields for other regions. A small component corresponding to the $h/2e$-periodicity in Figure 2B was also observed. In ref. 18 with Sb-doped $Bi_2Se_3$ TI nanoribbons, the observed $h/2e$ periodicity was

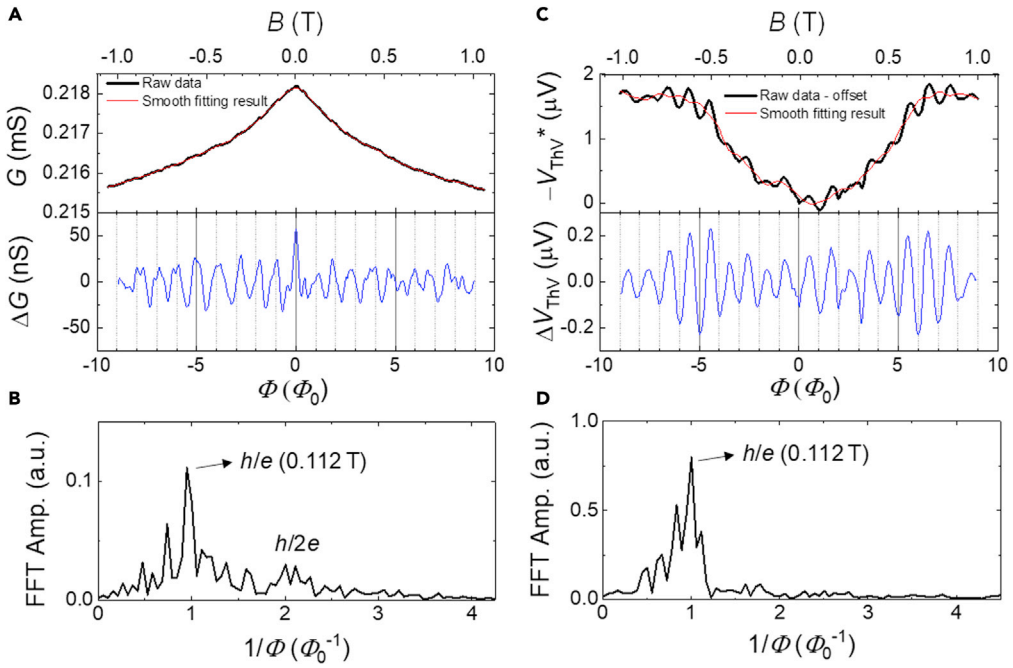


**Figure 2. Magnetoconductance and magnetothermovoltage oscillations of BiSe#1**

(A) Upper panel: conductance ($G$) as a function of magnetic flux ($\Phi$, bottom axis) (black curve) and the smooth fitting result (red curve) at $V_g$ = 0 V and $T$ = 4.2 K. Here, $\Phi$ is the magnetic flux normalized by the magnetic flux quantum, $\Phi_0$. Top axis: $B$ field. Lower panel: conductance difference between the raw data and smooth fitting result in the upper panel ($\Delta G$) as a function of $\Phi$.

(B) FFT amplitude of $\Delta G(\Phi)$ curve.

(C) Upper panel: $-V_{ThV}$* as a function of $\Phi$ (black curve) and smooth fit result (red one) at $V_g$ = 0 V and $T$ = 4.2 K. Lower panel: thermovoltage difference between the $-V_{ThV}$* ($\Phi$) curve and smooth fit result in the upper panel ($\Delta V_{ThV}$) as a function of $\Phi$.

(D) FFT amplitude of $\Delta V_{ThV}$ ($\Phi$) curve. In (A) and (C), we performed the smooth fitting of the raw data by using the Savitzky-Golay method with neighbor 50 points for a point.

interpreted as the Altshuler–Aronov–Spivak (AAS) oscillations, based on the analysis of temperature and gate-voltage dependences for various channel lengths, compared to the Aharonov-Bohm (AB) $h/e$ oscillations. In the study, it was found that the AAS oscillations were suppressed when the perimeter length ($L_p$) of the nanowire is shorter than the channel length ($L$) because a complete pair of the time-reversed paths was not formed along the perimeter of the nanowire in that case. On the other hand, in ref. 19, the observed $h/2e$ was explained by the interference of electrons that travel around the circumference of the TI NW two times in a quasi-ballistic regime, based on the exponential decay of the interference amplitude with increasing temperature. In our case, the channel length ($L$ = 6.8 μm) was much longer than the perimeter of the nanowire ($L_p \approx$ 1 μm), which indicates that our nanowire is closed to a diffusive limit allowing the complete formation of the time-reversed path along the perimeter of the NW to observe the AAS oscillations. The lower panel of Figure 2A shows the $h/2e$ oscillation only in a weak $B$-field region of $-\Phi_0<\Phi<\Phi_0$. The AAS oscillations are usually suppressed with increasing field because it needs a coherent backscattering condition under the time-reversal symmetry, which is broken at a sufficiently high $B$ field. Thus, we consider that the $h/2e$ oscillation observed in the magnetoconductance is related to the AAS oscillations.

We here address the variation of the thermovoltage with the $B$ field. The upper panel of Figure 2C shows $-V_{ThV}$* as a function of the $B$ field (black curve) at $V_{heater}$ = 100 mV, $V_g$ = 0 V, and $T$ = 4.2 K (see the raw data in Figure S1B of the Supplementary Information). The magnetothermovoltage also shows oscillation behavior under a varying $B$ field. After subtracting the smooth fitting result (red curve) from the raw data, we plotted the result [$\Delta V_{ThV}$ as a function of the $B$ field (top axis)] in the lower panel of Figure 2C. For the magneto-thermovoltage case, the FFT analysis provides an oscillation period of $\Delta B$ = 0.112 T (Figure 2D), which is consistent with that for the magnetoconductance oscillation. The magnetothermovoltage shows an even function of the $B$ field [e.g., $S(B) = S(-B)$], which is attributed to the invariant system when the $B$-field

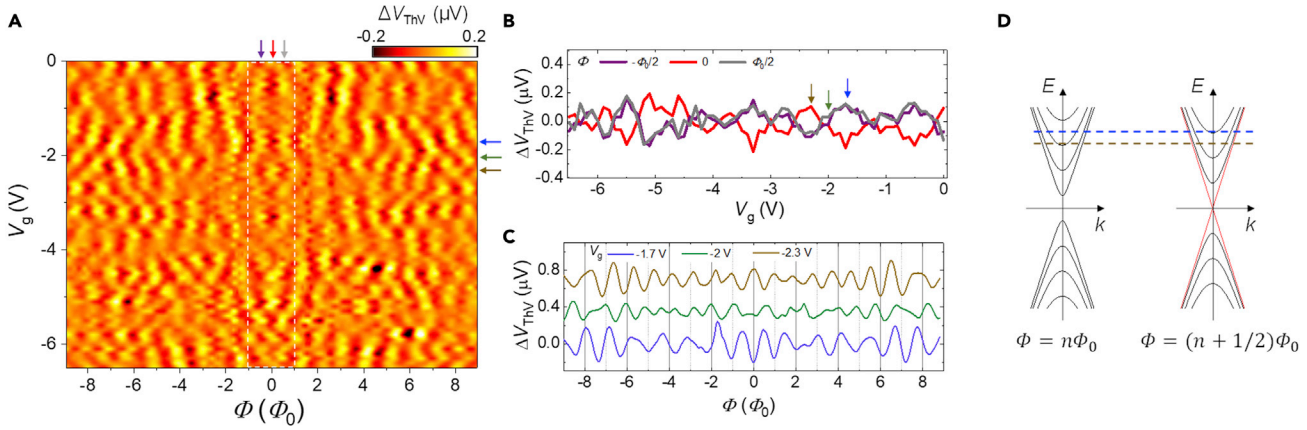


**Figure 3. 180° out-of-phase oscillations depending on the magnetic flux and gate voltage**

(A) $\Delta V_{ThV}$ as a function of $\Phi$ and $V_g$ of BiSe#1.

(B) $\Delta V_{ThV}$ as a function of $V_g$ at $\Phi = 0$ and $\pm\Phi_0/2$, where locations are also indicated by the same-colored arrows in (A).

(C) $\Delta V_{ThV}$ as a function of $\Phi$ at $V_g = -1.7$, $-2$, and $-2.3$ V; the corresponding locations are also indicated by the same-colored arrows in (A) and (B). Curves were vertically shifted for the clarity.

(D) Electronic sub-band dispersion at $\Phi = n\Phi_0$ and $(n + 1/2)\Phi_0$, where $n$ is an integer.

direction changes.[22] For the magnetothermovoltage oscillation case, the $\Delta V_{ThV}$ minima in the oscillation are located at integer multiples of $\Phi_0$ for the examined $\Phi$, without the FFT amplitude corresponding to the $h/2e$ oscillation (see Figure 2D). For the topmost NW segment in Figure 1A (BiSe#2), we also obtained similar behaviors in the magnetoconductance and magnetothermovoltage with similar periodicities (see Figure S2 in the Supplementary Information).

## Gate-voltage and magnetic-field dependences of the thermovoltage

Figure 3A displays $\Delta V_{ThV}$ as a function of $\Phi$ and $V_g$ for BiSe#1, which shows symmetric oscillations with respect to the zero field for the examined $V_g$ region (also see Figure S3 in the Supplementary Information for a different $V_g$ region). Near $\Phi = 0$, as indicated by a dashed white box, the patterns show oscillation behaviors for varying $V_g$. Figure 3B shows $\Delta V_{ThV}$ as a function of $V_g$ at $\Phi = -\Phi_0/2$, 0, and $\Phi_0/2$; these locations are indicated by vertical purple, red, and gray arrows in Figure 3A, respectively. The curve at $\Phi = 0$ shows a 180° out-of-phase modulation with respect to the two curves at $\Phi = \pm\Phi_0/2$, whereas the two curves show nearly the same modulation. This result is consistent with the sub-band model for the topologically protected surface state (TPSS) for a TI NW. In Figure 3D, the sub-band structures for $\Phi = n\Phi_0$ and $(n + 1/2)\Phi_0$ are plotted with a dispersion relation of $E(k, l, \Phi) = \pm\hbar v_F\sqrt{k^2 + \Delta k^2(l + 0.5 - \Phi/\Phi_0)^2}$, where $n$ is an integer, $\hbar$ is the reduced Planck's constant, $v_F$ is the Fermi velocity in the surface state, $k$ is the NW axial wave number, and $l$ (=0, $\pm1$, $\pm2$, ...) is the angular momentum quantum number; $\Delta k$ ( $= 2\pi/C$) is the quantized wave number along the perimeter of the TI NW, where $C$ is the circumference of the TI NW.[23,24] The cases of $\Phi = 0$ and $\pm\Phi_0/2$, i.e., n = 0 correspond to the left and right panels of Figure 3D, respectively. The dashed brown and blue lines indicate Fermi levels that meet the bottom of each sub-band for $\Phi = 0$ and $\pm\Phi_0/2$, respectively. Whenever the Fermi level crosses the sub-band with increasing $V_g$, the DOS shows a local maximum because of the flat bottom of each sub-band. The sub-band energy spacing at both $\Phi = 0$ and $\pm\Phi_0/2$ is determined by $\Delta E = \hbar v_F \Delta k$, where $v_F = 3 \times 10^5$ m s$^{-1}$ and $C = 1026$ nm (i.e., ~1.2 meV).

Because the Fermi level aligns with the bottom of sub-bands for the cases $\Phi = 0$ and $\pm\Phi_0/2$ in a 180° out-of-phase manner, the local maximum in the DOS is expected to alternatively appear as the $V_g$ is varied. The thermoelectric effect is sensitive to the change of the DOS in energy; thus, the 180° out-of-phase modulation behaviors in the thermovoltage with varying $V_g$ for cases of $\Phi = 0$ and $\pm\Phi_0/2$ in Figure 3C directly originate from the 180° out-of-phase behavior of the DOS with varying $V_g$ for the two cases. The two locations at $V_g = -2.3$ and $-1.7$ V indicated by brown and blue arrows in Figure 3B indicate the local magnetothermovoltage maxima for the cases of $\Phi = 0$ and $\pm\Phi_0/2$, respectively (see also the same-colored arrows in Figure 3A). In Figure 3C, the $\Delta V_{ThV}$ ($\Phi$) curves show a local maximum and minimum at $\Phi = 0$ for $V_g = -2.3$ and $-1.7$ V, which correspond to the Fermi energy locations, as indicated by dashed brown and

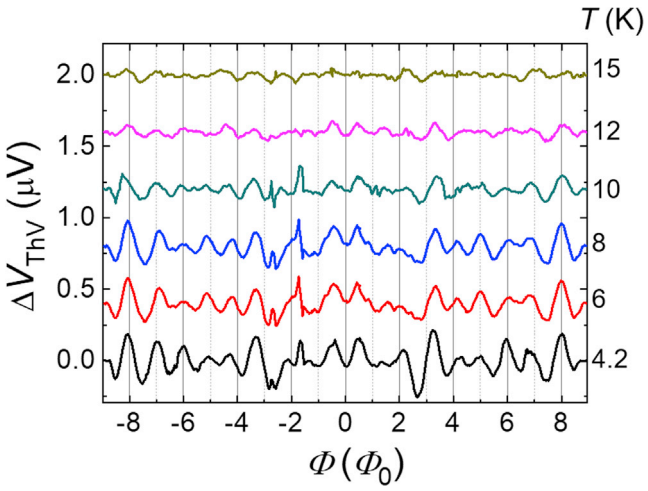


**Figure 4. Temperature dependence of magnetothermovoltage oscillations**

$\Delta V_{ThV}$ as a function of $\Phi$ at $V_g$ = 0 V for various temperatures (BiSe#1). Curves were vertically shifted for the clarity.

blue lines in Figure 3D, respectively. As $\Phi$ increases to $\Phi \sim \pm 2\Phi_0$, the thermovoltage modulation follows the prediction; for instance, local maxima and minima appear at even and odd multiples of $\pm \Phi_0/2$, which are known as AB oscillations with zero and $\pi$ phases (0-ABO and $\pi$-ABO), respectively.[19] For $2\Phi_0 < |\Phi| < 4\Phi_0$, the local maximum and minimum locations in the oscillations at $V_g$ = −2.3 and −1.7 V deviate slightly from those observed in $-2\Phi_0 < \Phi < 2\Phi_0$, possibly because of an additional de-phasing effect in a strong spin–orbit-coupled system.[19] However, at $V_g$ = −2 V indicated by the green arrow in Figures 3A and 3B, the oscillation pattern in Figure 3C shows a weakened oscillation amplitude with a non-regular period even at $-2\Phi_0 < \Phi < 2\Phi_0$, which is attributed to the regime being an intermediate state between the 0-ABO and $\pi$-ABO states. These behaviors were also observed in a relatively high $V_g$ region of 27–30 V, as shown in Figure S1 of the Supplementary Information. For the direct comparison between the magnetoconductance and magnetothermovoltage as a function of $V_g$ and $\Phi$, we prepared another BiSe NW (BiSe#3) and displayed the corresponding datasets in Figures S4–S6 of the Supplementary Information.

## Temperature dependences of magnetothermovoltage

Figure 4 shows $\Delta V_{ThV}$ as a function of $\Phi$ at various temperatures at $V_g$ = 0 V with BiSe#1, where the amplitude of the ABO is suppressed with increasing temperature, whereas the oscillation behavior is maintained even at $T$ = 15 K. We note that all $\Delta V_{ThV}$ ($\Phi$) curves showed the $\pi$ –ABO with the minimum value at $\Phi$ = 0, contrary to the observations at $V_g$ = 0 V in Figures 2 and 3. This implies that the intrinsic doping level changed. Actually, the temperature dependences were measured after performing the $\Delta V_{ThV}$ ($\Phi$) measurements in a range of 27–30 V for ~15 h, as shown in Figure S1 of the Supplementary Information. We consider that such high gate biasing for a relatively long period could induce a doping effect to the NW because of charge traps in the $SiO_2$ oxide layer,[25] resulting in a shift of the Fermi level compared to the that before applying such high $V_g$ condition. Because the temperature difference ($\Delta T$) between two different points in the relation of $S = -V_{ThV}/\Delta T$ changes as the base temperature is varied, the direct comparison of $-V_{ThV}$ at different temperatures could not provide a physical meaning. Nevertheless, it is clear that the phase coherence was kept to $T$ = 15 K without a transition between $\pi$-ABO and 0-ABO with increasing temperature, which indicates that the surface protected surface state may not experience de-phasing by disorder up to the 15 K.[19,23] In Figure S7 of the Supplementary Information, we also direct compared the magnetoconductance and magnetothermovoltage for varying temperatures with BiSe#3.

## Conclusions

We performed thermoelectric measurements for an Sb-doped $Bi_2Se_3$ NW to reveal the variation of the DOS at the Fermi level of topologically protected surface states when $\Phi$, $V_g$, and $T$ were varied. The thermovoltage oscillations with varying $V_g$ at $\Phi = 0$ and $\pm 2\Phi_0$ showed 180° out-of-phase behavior,

which indicates that surface-state sub-bands because of the confinement along the perimeter of the TI NW exist at the NW surface. The magnetothermovoltage obtained at two $V_g$ values showing local maximum and minimum thermovoltage values at $\Phi = 0$ also showed the 180° out-of-phase modulation behavior, as expected on the basis of the $\Phi$-dependent sub-band dispersion model. Thus, thermoelectric measurements could be used to reveal the electronic structure at the Fermi level for various quantum materials.

### Limitations of the study

In previous studies, thermoelectric measurements were conducted by measurement of the Seebeck coefficient $S$. In the present study, however, we performed the thermoelectric measurement in terms of the thermovoltage because we did not have metallic thermometers for the NW. Consequently, to justify the $T$-dependence of the thermovoltage, we estimated $\Delta T$ at the examined temperatures with another device having the same geometrical conditions but with metallic thermometers.

## STAR★METHODS

Detailed methods are provided in the online version of this paper and include the following:

- KEY RESOURCES TABLE
- RESOURCE AVAILABILITY
  - Lead contact
  - Material availability
  - Data and code availability
- EXPERIMENTAL MODEL AND SUBJECT DETAILS
- METHOD DETAILS
  - Synthetic method
  - Device fabrication
  - Measurements

## SUPPLEMENTAL INFORMATION

Supplemental information can be found online at https://doi.org/10.1016/j.isci.2022.105691.

## ACKNOWLEDGMENTS

This work was supported by the National Research Foundation funded by the Korea Government (Grant Nos. 2016R1A5A1008184, 2018R1A2A1A05078440, 2018R1A3B1052827, 2021R1A2C3012612, 2020R1A6A1A03047771, 2022M3H4A1A04074153, 2020R1A2C1011000) and the Korea Research Institute of Standards and Science (KRISS-2022-GP2022-0001). This work was also supported by Korea Institute for Advancement of Technology (KIAT) grant funded by the Korea Government (MOTIE) (P0008458, The Competency Development Program for Industry Specialist).

## AUTHOR CONTRIBUTIONS

M.B. and J.S. conceived the experiments. D.K. fabricated the device and performed the measurements with B.K. D.Y. grew the Sb-doped $Bi_2Se_3$ nanowires and Y.D. helped with the analysis. All authors discussed the results and contributed to the writing of the manuscript.

## DECLARATION OF INTERESTS

The authors declare no competing interests.

Received: August 2, 2022
Revised: November 9, 2022
Accepted: November 28, 2022
Published: January 5, 2023

## REFERENCES


1. Chen, I.J., Burke, A., Svilans, A., Linke, H., and Thelander, C. (2018). Thermoelectric power factor limit of a 1D nanowire. Phys. Rev. Lett. *120*, 177703. https://doi.org/10.1103/PhysRevLett.120.177703.

2. Zhao, M., Kim, D., Lee, Y.H., Yang, H., and Cho, S. (2022). Quantum sensing of thermoelectric power in low-dimensional materials. Adv. Mater. 2106871. https://doi.org/10.1002/adma.202106871.

3. Mao, J., Liu, Z., and Ren, Z. (2016). Size effect in thermoelectric materials. NPJ Quantum Mater. *1*, 16028. https://doi.org/10.1038/npjquantmats.2016.28.

4. Dresselhaus, M.S., Chen, G., Tang, M.Y., Yang, R.G., Lee, H., Wang, D.Z., Ren, Z.F., Fleurial, J.-P., and Gogna, P. (2007). New directions for low-dimensional thermoelectric materials. Adv. Mater. *19*, 1043–1053. https://doi.org/10.1002/adma.200600527.

5. Ichinose, Y., Matsubara, M., Yomogida, Y., Yoshida, A., Ueji, K., Kanahashi, K., Pu, J., Takenobu, T., Yamamoto, T., and Yanagi, K. (2021). One-dimensionality of thermoelectric properties of semiconducting nanomaterials. Phys. Rev. Mater. *5*, 025404. https://doi.org/10.1103/PhysRevMaterials.5.025404.

6. Hamdou, B., Gooth, J., Böhnert, T., Dorn, A., Akinsinde, L., Pippel, E., Zierold, R., and Nielsch, K. (2015). Thermoelectric properties of band structure engineered topological insulator $(Bi_{1-x}Sb_x)_2Te_3$ Nanowires. Adv. Energy Mater. *5*, 1500280. https://doi.org/10.1002/aenm.201500280.

7. Nikolaeva, A.A., Konopko, L.A., Huber, T.E., Bodiul, P.P., and Popov, I.A. (2012). Prospects of nanostructures $Bi_{1-x}Sb_x$ for thermoelectricity. J. Solid State Chem. *193*, 71–75. https://doi.org/10.1016/j.jssc.2012.03.063.

8. Xu, N., Xu, Y., and Zhu, J. (2017). Topological insulators for thermoelectrics. NPJ Quantum Mater. *2*, 51. https://doi.org/10.1038/s41535-017-0054-3.

9. Dedi, Lee, P.-C., Wei, P.-C., and Chen, Y.-Y. (2021). Thermoelectric characteristics of a single-crystalline topological insulator $Bi_2Se_3$ nanowire. Nanomaterials *11*, 819.

10. Ashalley, E., Chen, H., Tong, X., Li, H., and Wang, Z.M. (2015). Bismuth telluride nanostructures: preparation, thermoelectric properties and topological insulating effect. Front. Mater. Sci. *9*, 103–125. https://doi.org/10.1007/s11706-015-0285-9.

11. Konopko, L., Nikolaeva, A., Huber, T.E., and Rogacki, K. (2020). Quantum oscillations in nanowires of topological insulator $Bi_{0.83}Sb_{0.17}$. Appl. Surf. Sci. *526*, 146750. https://doi.org/10.1016/j.apsusc.2020.146750.

12. Cho, S., Kang, S.D., Kim, W., Lee, E.-S., Woo, S.-J., Kong, K.-J., Kim, I., Kim, H.-D., Zhang, T., Stroscio, J.A., et al. (2013). Thermoelectric imaging of structural disorder in epitaxial graphene. Nat. Mater. *12*, 913–918. https://doi.org/10.1038/nmat3708.

13. Lee, E.-S., Cho, S., Lyeo, H.-K., and Kim, Y.-H. (2014). Seebeck effect at the atomic scale. Phys. Rev. Lett. *112*, 136601. https://doi.org/10.1103/PhysRevLett.112.136601.

14. Gofryk, K., Griveau, J.C., Riseborough, P.S., and Durakiewicz, T. (2016). Thermoelectric power as a probe of density of states in correlated actinide materials: the case of $PuCoGa_5$ superconductor. Phys. Rev. B *94*, 195117. https://doi.org/10.1103/PhysRevB.94.195117.

15. Choi, S.J., Kim, B.-K., Lee, T.-H., Kim, Y.H., Li, Z., Pop, E., Kim, J.-J., Song, J.H., and Bae, M.-H. (2016). Electrical and thermoelectric transport by variable range hopping in thin black phosphorus devices. Nano Lett. *16*, 3969–3975. https://doi.org/10.1021/acs.nanolett.5b04957.

16. Ning, W., Du, H., Kong, F., Yang, J., Han, Y., Tian, M., and Zhang, Y. (2013). One-dimensional weak antilocalization in single-crystal $Bi_2Te_3$ nanowires. Sci. Rep. *3*, 1564. https://doi.org/10.1038/srep01564.

17. Kim, J., Lee, S., Brovman, Y.M., Kim, M., Kim, P., and Lee, W. (2014). Weak antilocalization and conductance fluctuation in a single crystalline Bi nanowire. Appl. Phys. Lett. *104*, 043105. https://doi.org/10.1063/1.4863421.

18. Kim, H.-S., Hwang, T.-H., Kim, N.-H., Hou, Y., Yu, D., Sim, H.S., and Doh, Y.-J. (2020). Adjustable quantum interference oscillations in Sb-doped $Bi_2Se_3$ topological insulator nanoribbons. ACS Nano *14*, 14118–14125. https://doi.org/10.1021/acsnano.0c06892.

19. Jauregui, L.A., Pettes, M.T., Rokhinson, L.P., Shi, L., and Chen, Y.P. (2016). Magnetic field-induced helical mode and topological transitions in a topological insulator nanoribbon. Nat. Nanotechnol. *11*, 345–351. https://doi.org/10.1038/nnano.2015.293.

20. Kim, M., Kim, J., Hou, Y., Yu, D., Doh, Y.-J., Kim, B., Kim, K.W., and Suh, J. (2019). Nanomechanical characterization of quantum interference in a topological insulator nanowire. Nat. Commun. *10*, 4522. https://doi.org/10.1038/s41467-019-12560-4.

21. Peng, H., Lai, K., Kong, D., Meister, S., Chen, Y., Qi, X.-L., Zhang, S.-C., Shen, Z.-X., and Cui, Y. (2010). Aharonov–Bohm interference in topological insulator nanoribbons. Nat. Mater. *9*, 225–229. https://doi.org/10.1038/nmat2609.

22. Yang, N.-X., Zhou, Y.-F., Lv, P., and Sun, Q.-F. (2018). Gate voltage controlled thermoelectric figure of merit in three-dimensional topological insulator nanowires. Phys. Rev. B *97*, 235435. https://doi.org/10.1103/PhysRevB.97.235435.

23. Bardarson, J.H., Brouwer, P.W., and Moore, J.E. (2010). Aharonov-Bohm oscillations in disordered topological insulator nanowires. Phys. Rev. Lett. *105*, 156803. https://doi.org/10.1103/PhysRevLett.105.156803.

24. Zhang, Y., and Vishwanath, A. (2010). Anomalous Aharonov-Bohm conductance oscillations from topological insulator surface states. Phys. Rev. Lett. *105*, 206601. https://doi.org/10.1103/PhysRevLett.105.206601.

25. Huang, X., Yao, Y., Peng, S., Zhang, D., Shi, J., and Jin, Z. (2020). Effects of charge trapping at the $MoS_2$–$SiO_2$ interface on the stability of subthreshold swing of $MoS_2$ field effect transistors. Materials *13*, 2896. https://doi.org/10.3390/ma13132896.

## STAR★METHODS

### KEY RESOURCES TABLE

| REAGENT or RESOURCE | SOURCE | IDENTIFIER |
|---|---|---|
| Chemicals, peptides, and recombinant proteins | | |
| $Bi_2Se_3$ powder (99.999%) | Alfa Aesar | 13126 |
| Sb powder (99.999%) | Alfa Aesar | 14640 |
| Se powder (99.999%) | Alfa Aesar | 10603 |
| Ti pellets | ITASCO | 7440-32-6 |
| Au pellets | ITASCO | 7440-57-5 |
| Software and algorithms | | |
| Origin 2019b | Origin Lab | https://www.originlab.com/ |

### RESOURCE AVAILABILITY

#### Lead contact

Further information and requests for resources should be directed to and will be fulfilled by the lead contact, Dr. Myung-Ho Bae (mhbae@kriss.re.kr).

#### Material availability

This study did not generate new unique reagents.

#### Data and code availability

- Data reported in this paper will be shared by the lead contactupon request.
- There is no dataset or code associated with this work.
- Gate-dependent magnetoconductance (magnetothermovoltage), Temperature-dependent magneconductance (magnetothermovoltage)

### EXPERIMENTAL MODEL AND SUBJECT DETAILS

This study does not use experimental methods typical in the life sciences.

### METHOD DETAILS

#### Synthetic method

$Bi_{2-x}Sb_xSe_3$ nanoribbons (x ranging from 0.15 to 0.4) were grown by a chemical vapor deposition (CVD) method in a Lindberg Blue M tube furnace. $Bi_2Se_3$ powder (99.999%, Alfa Aesar) mixed with Sb powder (99.999%, Alfa Aesar) was placed at the center of the tube, whileSe pellets (99.999%, Alfa Aesar) were placed upstream at 16 cm from the center. A silicon substrate coated with a 10 nm Au film was placed downstream 14 cm from the center. During the 5 h of growth time, the temperature of the furnace was maintained at 680 °C, Argon flow rate was kept at a 150 sccm, and the pressure was maintained at room pressure. The furnace was then cooled down to room temperature over approximately 3 h.

#### Device fabrication

Sb-doped $Bi_2Se_3$ NWs were synthesized on a Si substrate in a tube furnace via the chemical vapor deposition method. A selected Sb-$Bi_2Se_3$ NW was mechanically transferred using a tungsten tip onto a Si substrate covered with a 290 nm-thick $SiO_2$ layer. For the electrical measurement, we deposited contact metal Ti/Au (thickness: 160/50 nm) using electron (e)-beam lithography and e-beam evaporation. Before the e-beam evaporation, e-beam resist residue and the native oxide layer on the surface of the NWs were removed using an $O_2$ plasma asher (power: 200 W, time: 80 s) and by dipping into a 6:1 buffered oxide etchant for 10 s, respectively.

### Measurements

Electrical measurements for the NWs were performed using the two-probe scheme with a lock-in system (frequency: 21.77 Hz, ac current: 50 nA) with the sample in a liquid $^4$He system equipped with a 9 T magnet. Thermovoltage measurements were conducted with a nanovoltmeter in DC mode with a DC heater voltage.